Available online at www.sciencedirect.com

ScienceDirect

Advances in Space Research xxx (xxxx) xxx

ADVANCES IN SPACE RESEARCH (a COSPAR publication)

www.elsevier.com/locate/asr

High-precision physics-based radiation force models for the Galileo spacecraft

Santosh Bhattarai [a,*], Marek Ziebart [a], Tim Springer [b], Francisco Gonzalez [c] Guillermo Tobias [d]

[a] Department of Civil, Environmental and Geomatic Engineering, University College London, UK
[b] PosiTim UG, Seeheim-Jugenhein, Germany
[c] European Space Agency, ESA/ESTEC, Noordwijk, The Netherlands
[d] GMV, Madrid, Spain

Received 9 February 2022; received in revised form 30 March 2022; accepted 1 April 2022

Abstract

We present two new high-precision physics-based radiation force models for the In-Orbit Validation (IOV) and Full Operational Capability (FOC) spacecraft (s/c) of the Galileo Global Navigation Satellite System (GNSS). In both cases, the s/c bus surfaces are covered in material types, i.e., Laser Retro-reflector Array (LRA), Optical Surface Reflector (OSR) and Single-Layer Insulation (SLI) coverings, that were either not encountered or not specifically dealt with in earlier work. To address this, a number of modelling enhancements were proposed and tested, including: a specific model to account for the direct and reflected solar radiation force for LRA surfaces; a design update of the bus model computation process to allow for more than one insulation material; a specific thermal force model for OSR surfaces; a thermal force model for the Navigation Antenna (NAVANT) surface that includes a temperature model derived from on-orbit temperature measurements; and force models to account for thermal emissions from radiator panels on the +X and ±Y surfaces for both IOV and FOC, and on the −Z surface for FOC only. In the UCL2+ model each of these effects are accounted for. The theoretical impact of each modelling concept introduced is assessed, individually, by considering the magnitude of its effect in acceleration-space. The impact on orbit accuracy is confirmed through a rigorous set of Precise Orbit Determination (POD) validation tests, in which observations from all active Galileo s/c over two full years, 2017 and 2018, including during eclipsing periods, are included in the analysis. The UCL2+ approach results in day boundary discontinuities of 22 mm, 17 mm and 27 mm in the radial, across-track and along-track components, respectively. Analysis of the one-way Satellite Laser Ranging (SLR) residuals suggests that radial accuracy at better than 1 cm (3.7 mm mean residuals) and precision at better than 2 cm (17 mm root mean square (rms) error) is achievable with the UCL2+ model.

Keywords: Radiation force modelling; Precise orbit determination; Galileo; In-orbit validation; Full operational capability; Global Navigation Satellite Systems (GNSS)

1. Introduction

The radiation force modelling problem is the major issue that must be dealt with in order to accurately determine the position of Global Navigation Satellite System (GNSS) satellites at the centimetre-level. In the GNSS literature,

* Corresponding author at: Department of Civil, Environmental and Geomatic Engineering, University College London, UK, email: s.bhattarai@ucl.ac.uk
E-mail address: s.bhattarai@ucl.ac.uk (S. Bhattarai).

https://doi.org/10.1016/j.asr.2022.04.003
0273-1177/

Acronyms & Abbreviations

BFS	Body-Fixed System
BW + R	Box-Wing + Re-radiation
CODE	Centre for Orbit Determination in Europe
ECOM	Empirical CODE Orbit Model (9 parameters)
ECOM-1	Empirical CODE Orbit Model (5 of 9 parameters estimated)
ECOM-2	Extended (4 extra parameters in D) ECOM (7 or 9 of 13 parameters estimated)
EPS	Earth-Probe-Sun
ERP	Earth Radiation Pressure
EUSPA	European Union Agency of the Space Programme
FOC	Full Operational Capability
GNSS	Global Navigation Satellite System
IOV	In-Orbit Validation
IERS	International Earth rotation and Reference systems Service
IP	Intersection Point
JPL	Jet Propulsion Laboratory
LRA	Laser Retro-reflector Array
MLI	Multi-layer Insulation
OSR	Optical Surface Reflector
NAVANT	Navigation Antenna
POD	Precise Orbit Determination
s/c	spacecraft
SLI	Single-layer Insulation
SLR	Satellite Laser Ranging
SM	Standard Surface Material
SRP	Solar Radiation Pressure
STC	Analytical SRP & TRR modelling Software Classic
TRP	Thermal Reference Point
TRR	Thermal Re-radiation

methods for dealing with this problem are classified as analytical (or physics-based) (Ziebart 2004; Li et al. 2018; Darugna et al. 2018; Bhattarai et al. 2019); empirical (Beutler et al. 1994; Springer et al. 1999; Bar-Sever and Kuang 2003; Arnold et al. 2015); or as a hybrid approach belonging somewhere on a spectrum between the two (Rodriguez-Solano et al. 2012; Montenbruck et al. 2017a). This classification scheme is useful insofar as it describes, in broad terms, the modelling approaches developed and used by different groups working on GNSS precise orbit determination (POD). We shall also characterise the work presented in this paper according to this scheme. Readers interested in a detailed description of these distinct modelling philosophies, and how they have emerged, accompanied by discussions about their limitations and benefits, will find the sources we cite in this section a good place to start.

Focussing on the Galileo system, for this study, we develop several enhancements to the high precision analytical approach that uses detailed *a priori* physics-based models of radiation forcing in the POD process, and systematically investigate the impact of the proposed enhancements on orbit accuracy. In the high precision approach, the broad objective is to use all available knowledge about the spacecraft (e.g., surface geometry, surface material properties, attitude, spacecraft thermal control mechanisms, etc.) and its operating environment to construct the model. The model's purpose is to account for the effect of photon flux through all surfaces on the position and trajectory of the space vehicle. We refer to the models as high precision (or high fidelity) to distinguish them from the relatively simpler cannonball or box-wing class of analytical models.

There is good evidence to suggest that including *a priori* knowledge about surface geometry and material properties in the POD process can improve orbit accuracy. An early study exploring POD performance using the Galileo IOV satellites found that the Centre for Orbit Determination in Europe's (CODE's) Empirical CODE Orbit Model (ECOM-1; Springer et al. 1999) could not adequately capture the effects of solar radiation pressure (SRP) on a spacecraft with an oblong-shaped bus. Introducing an *a priori* cuboid box model to represent the bus addressed this problem, to an extent, reducing peak radial errors outside eclipse periods from 20 cm down to 5 cm (Montenbruck et al. 2015). In a series of more recent studies, Galileo s/c metadata (surface geometry and material properties) published by the European Union Agency of the Space Programme (EUSPA) was used construct box-wing models of the IOV and FOC s/c (Bury et al. 2019). These were used for *a priori* modelling of radiation forcing in a hybrid POD processing scheme that included the Extended Empirical CODE Orbit Model (ECOM-2; Arnold et al. 2015). Various modelling strategies were tested using one-way SLR residuals analysis with results indicating that, for all Galileo satellites, including during eclipsing periods, best case radial accuracy (mean residuals) at 15.3 mm and best case precision (rms errors) at 22.5 mm is achievable, but with a trade-off between accuracy and precision (Bury et al. 2020).

In this paper, we present a high-precision physics-based radiation force modelling approach for the Galileo In-Orbit Validation (IOV) and Full Operational Capacity (FOC) spacecraft. The bus component of the model is published alongside the article. The other components of the model are fully described here or within the published literature. The overall modelling approach and the limitations

that it addresses are described in Section 2.2. The force model equations are presented in Section 3. In Section 3.8, we present an analysis of the impact of the modelling concepts introduced in the acceleration-space. The data sources used to build the IOV and FOC s/c models are described in Section 4. In Section 5, we describe a series of POD validation tests and assess the results by analysing the day-boundary discontinuities (Section 5.1) and the SLR residuals (Section 5.2). We summarise our conclusions and discuss their implications in Section 6.

2. The UCL modelling strategy

To a large extent, the radiation force models developed for this study are produced using methods described in Bhattarai et al. (2019), where the complete model comprises the output of three separate modelling processes dealing with the s/c bus, the solar panels and antenna thrust. Here, the novel contributions deal primarily with updates to the processes for creating the s/c bus component of the radiation force model, which shall be referred to simply as the bus model henceforth. For a detailed description of the overall modelling strategy, see Section 2 of Bhattarai et al. (2019) and for details on how the models can be implemented in precise orbit determination (POD) algorithms, see Section 3 of the same article. The current process is an evolution of an approach for precision solar force modelling for GLONASS satellites presented in Ziebart and Dare (2001), which has since been enhanced with methods to account for thermal re-radiation (Ziebart et al. (2005), Earth radiation pressure (ERP; Sibthorpe 2006; Ziebart et al. (2007) and antenna thrust Ziebart et al. (2007). The approach has been validated on several cases including the GPS Block IIA and GPS Block IIR/IIR-M satellites (Ziebart et al. 2005; Bhattarai et al. 2019), ENVISAT (Sibthorpe 2006) and the Jason-1 satellite of the Ocean Surface Topography Mission (Cerri et al. 2010; Zelensky et al. 2010).

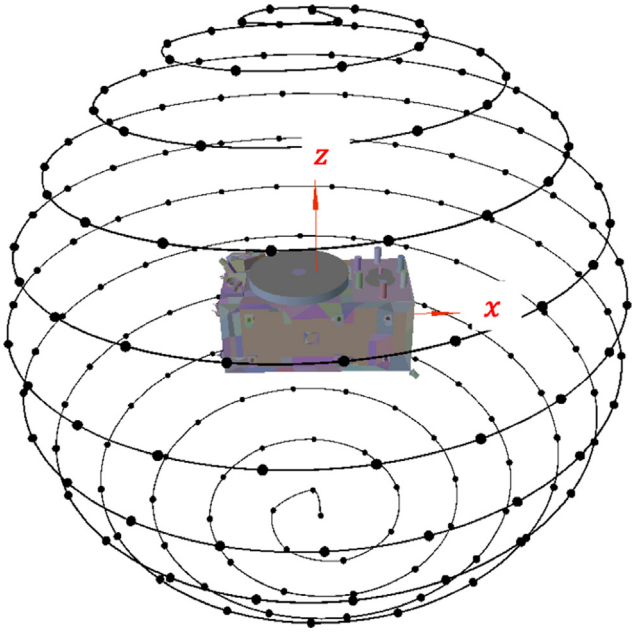

Fig. 1. A visualisation to explain the use of the spiral points algorithm in the bus model computation process, wherein UCL's model of the Galileo FOC s/c bus is surrounded by 200 spiral points. The standard bus model computation uses 10,000 spiral points.

2.1. Overview of the bus model computation process

As input, the process for computing the bus model requires information about the surface geometry and knowledge of certain surface material properties such as reflectivity, specularity and emissivity. A spiral points algorithm is used to systematically sample discrete points along a spiral path on a sphere surrounding the s/c model in an efficient manner (Saff and Kuijlaars 1997), as illustrated in Fig. 1 wherein UCL's model of the Galileo FOC s/c is surrounded by 200 spiral points. At each spiral point location, a pixel array simulates the planar wavefront of a distant radiation source. The centre of the pixel array represents the location of a radiation source in the s/c body-fixed system (BFS). A ray-tracing technique is then used to project the pixel array onto the s/c model, as shown in Fig. 2 (left). At each intersection point (IP), depicted by red dots in Fig. 2 (right), a material-dependent ray-surface interaction model (detailed in Sections 3.1–3.5) is used to compute the acceleration due to radiation forcing for the surface area element corresponding to that IP. The resultant acceleration is calculated as the sum of accelerations computed at each IP. This ray-tracing process is repeated at each spiral point location. The standard bus model computation uses 10,000 spiral points, which provides a high-resolution map of the accelerations induced by the ray-surface interactions from radiation source locations uniformly distributed around the s/c BFS. The outputs from the spiral point computations are combined using a 2-d inverse-distance weighted interpolation algorithm (Shepard 1968) to produce a set of three grids, one each for the x, y and z components of acceleration, with nodes spaced at $1^{\circ} \times 1^{\circ}$ intervals in latitude and longitude in the s/c BFS.

One of the main advantages of this computation process is that it produces a general-purpose force model, in that sense that all possible orientations of the radiation source in the s/c BFS are dealt with. However, during nominal operating conditions, for the Galileo s/c, the Sun is confined to the half-plane where $x < 0$ in the xz-plane of the s/c BFS, as shown in Fig. 3. In nominal conditions, the Earth-Probe-Sun angle, θ'_{EPS}, varies within the interval $(0, \pi)$. The sun does not directly shine upon the $+x$ or $\pm y$ surfaces. This is relevant as it informs various aspects of the model development and analysis work presented in later sections.

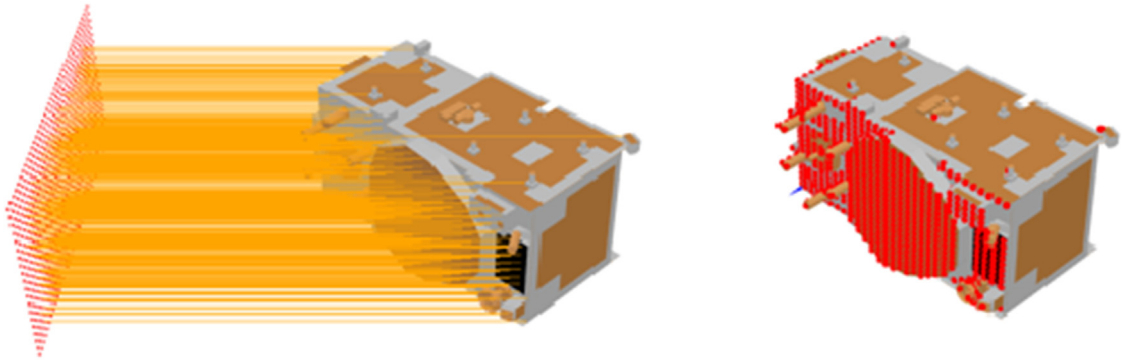

Fig. 2. A depiction of the ray-tracing technique. **Left:** A pixel array that simulates a radiation source, in a particular direction in the s/c BFS, is generated. Rays originate from the pixel centre points and project onto a computer model of the s/c. **Right:** At each intersection point, illustrated by red dots, where the rays meet the s/c surface, the force is computed according to Equations 1–6. The resultant force is the sum of forces computed at each intersection point.

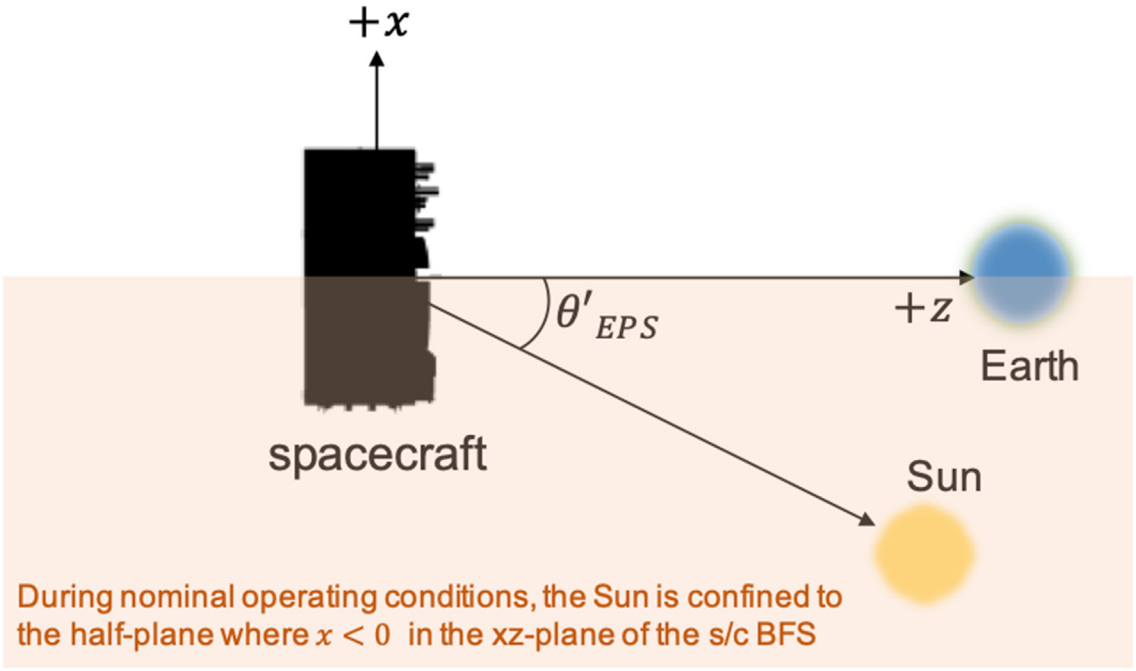

Fig. 3. A depiction of the Galileo s/c bus that shows the +x and +z axes of the s/c BFS. In nominal attitude mode, the +z BFS axis points to the geocenter and the Sun is confined to the region shaded in orange, i.e., the half-plane where $x < 0$ in the xz-plane.

2.2. Radiation force modelling for the Galileo s/c and the limitations of the existing approach

Prior to this work, the computation process considered two categories of materials in the ray-surface interaction equations: the standard material (SM) type and the multi-layer insulation (MLI) type. For both material types, the material-dependent ray-surface interaction equations account for the momentum transfer that occurs when radiation is absorbed, henceforth referred to as the direct solar force, and the reaction force that arises when radiation is reflected, either diffusely or in a specular manner, henceforth referred to as the reflected solar force.

For materials classified as MLI, the thermal re-radiation (TRR) force arising due to anisotropic thermal emissions is also considered, but the design of the computation process allowed for a single MLI material only. This was acceptable in previous studies where the development and validation of the MLI TRR effect was carried out in the context of the GPS Block IIR/IIR-M and Jason-1 Ocean Surface Topography Mission (OSTM) satellites (Adhya 2005; Ziebart et al. 2005; Bhattarai et al. 2019). In those cases, it was understood that there was a single MLI material type wrapped around the s/c bus for both spacecraft types. However, this is not the case for the Galileo s/c, where there are two types of insulation materials covering the

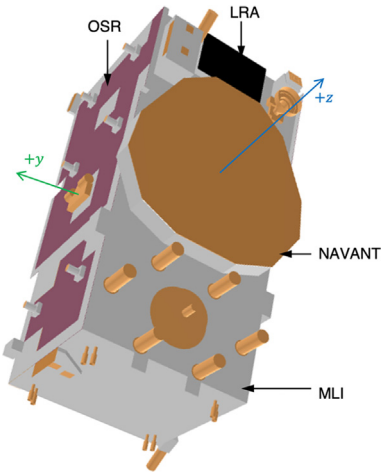

Fig. 4. A visualisation of the UCL s/c model of the Galileo IOV s/c bus showing the +y and +z BFS axes along with labels pointing to four surface material types considered in the radiation force model computations: MLI, OSR, LRA and NAVANT.

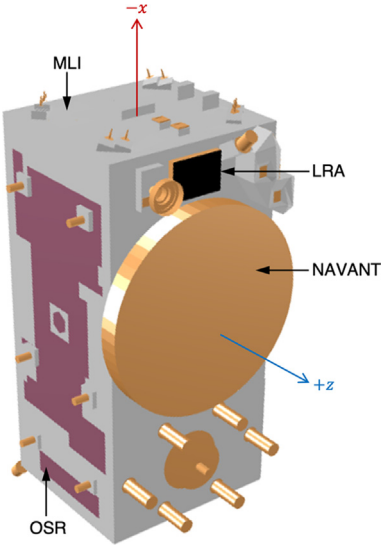

Fig. 5. A visualisation of the UCL s/c model of the Galileo FOC s/c bus showing the -x and +z BFS axes along with labels points to the surface material types considered in the radiation force model computations: MLI, OSR, LRA and NAVANT.

bus, i.e., single layer insulation (SLI) and MLI. Thus, it is appropriate to update the model computation process to deal with multiple insulation materials.

Additionally, both classes of s/c have a laser retroreflector array (LRA), comprised of corner cube reflectors (CCR) fixed onto a baseplate that is mounted on the +z-face of the bus, as shown in Fig. 4 and Fig. 5 for IOV and FOC, respectively. The purpose of the LRA is to enable satellite laser ranging (SLR), an accurate and independent measurement technique that is useful for orbit validation (e.g. Urschl et al. (2005)).

If we naively apply earlier modelling methods to LRA surfaces, the implicit assumption is that the LRA surfaces behave like conventional glass surfaces, in that incident radiation is specularly reflected according to the conventional law of reflection. In reality, CCRs are specifically designed to reflect light in the anti-parallel direction. Thus, the effects of the radiation-surface interaction between an LRA surface and the other surface material types are fundamentally different. Details of the direct and reflected solar force model, developed specifically to deal with LRA surfaces, are presented in Section 3.2 and the impact of the mismodelling of LRA surfaces as SM surfaces is evaluated in the acceleration-space in Section 3.8.

For the most part, for both IOV and FOC, the internal temperature of the s/c bus is passively maintained. The exception is the clock unit, located on the interior side of the +x face, which is actively kept at a set point temperature that is always higher than the equilibrium temperature. Excess heat generated by all payload and platform components is dissipated through parts of the s/c exterior surfaces that are covered in the optical surface reflector (OSR) material. Thus, for the OSR material, because its primary purpose is to facilitate heat dissipation from onboard components, we assume that all absorbed radiation is instantaneously re-radiated as heat. The OSR TRR model equations are presented in Section 3.4.

Finally, the thermal behaviour of the NAVANT, a heavy payload unit mounted onto the exterior side of the +z surface, which is thermally separated from interior of the s/c bus by an MLI surface covering requires careful consideration. The details of a NAVANT thermal force model that makes use of *in situ* temperature measurements are presented in Section 3.5.

3. Solar and thermal force model equations

For ALL surface material types, at each intersection point (IP) a ray-surface interaction model is used to compute the direct solar force and the recoil force due to reflected (diffuse and specular) radiation. For SOME surface material types, i.e., MLI and OSR, the thermal force is also considered. In this section, the specific solar and thermal force model equations developed for the Galileo IOV and FOC s/c are presented. Unless otherwise stated, these model equations are implemented within the ray-tracing computation process.

3.1. Solar force model for standard (or default) material surfaces

For SM surfaces, the force is computed according to:

$$\mathbf{F_n} = -W\left[(1+\mu v)\cos\theta + \frac{2}{3}v(1-\mu)\right]\hat{\mathbf{n}} \quad (1)$$

$$\mathbf{F_s} = W\sin\theta(1-\mu v)\hat{\mathbf{s}} \quad (2)$$

where $\mathbf{F_n}$ is the normal force acting in the direction of the surface normal, $\hat{\mathbf{n}}$; $\mathbf{F_s}$ is the shear force acting in the $\hat{\mathbf{s}}$ direction along the surface;v is the reflectivity of the material; μ is the specularity of the material; and:

$$W = \frac{EA}{c}\cos\theta \tag{3}$$

where E is the mean irradiance of the radiation source at 1 astronomical unit; A is the area of the surface element, c is the speed of light in vacuum; and θ is the angle of incidence.

3.2. Solar force model for LRA surfaces

For LRA surfaces, the normal component of the direct solar force, $\mathbf{F_n}$, is computed using Equation (1). The shear component of the direct solar force, $\mathbf{F_s}$, is computed according to:

$$\mathbf{F_s} = W\sin\theta(1+\mu v)\hat{\mathbf{s}} \tag{4}$$

where all terms in Equation (4) have been defined previously. The ray-surface interaction models for SM surfaces (top) and LRA surfaces (bottom) are illustrated in Fig. 6, where **s** represents incoming radiation, **r** represents specularly reflected radiation, $\mathbf{F}_\alpha$ denotes the direct force due to the absorbed radiation and $\mathbf{F_\mu}$ denotes the recoil force that arises due to specularly reflected radiation. The recoil force that arises due to diffusely reflected radiation is not depicted here as it is identical for both cases. The fundamental difference is that $\mathbf{F_\mu}\cdot\hat{\mathbf{s}}$, the shear component of $\mathbf{F_\mu}$, acts in opposite directions in these two cases. In the SM case, the shear components of $\mathbf{F}_\alpha$ and $\mathbf{F_\mu}$ point in opposite directions, reducing the magnitude of the shear component of the overall force. In the LRA case, the shear components of $\mathbf{F}_\alpha$ and $\mathbf{F_\mu}$ point in the same direction, reinforcing each other, and thus increasing the magnitude of the shear component of the overall force.

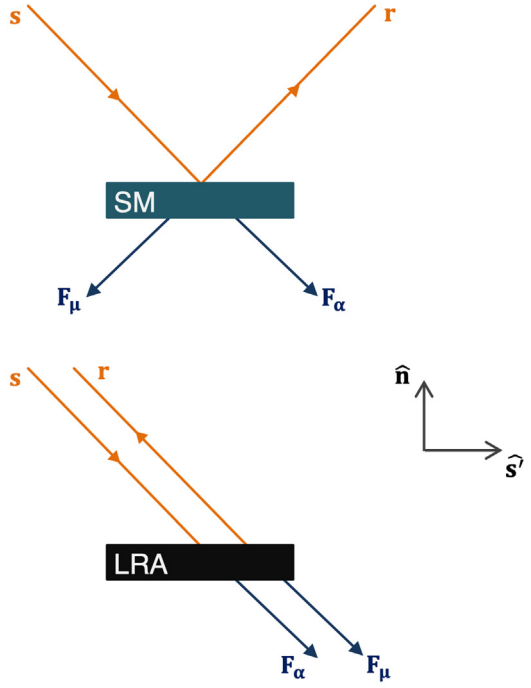

Fig. 6. An illustration depicting the difference between the ray-surface interaction model in the Standard Material case and the Laser Retroflector Array case. The fundamental difference is that the shear component, $\hat{s}'$, of the recoil force, $\boldsymbol{F_\mu}$, that arises due to the specularly reflected radiation acts in exactly the opposite direction, i.e., in the $-\hat{s}'$ direction in the SM case and in the $+\hat{s}'$ direction in the LRA case.

For both the IOV and FOC cases, we can gain valuable insight into the impact of mis-modelling LRA surfaces as SM surfaces by considering the difference between resultant accelerations given by the SM model and the resultant accelerations given by the LRA model. This acceleration change model is given by:

$$\Delta\mathbf{a_s} = \frac{\mathbf{F}_{\text{lra}} - \mathbf{F}_{\text{sm}}}{m} = \frac{2W\sin\theta\mu v}{m}\hat{\mathbf{s}} = \frac{EA\sin 2\theta\mu v}{mc}\hat{\mathbf{s}} \tag{5}$$

where $\Delta\mathbf{a_s}$ is the change in acceleration; $\mathbf{F}_{\text{lra}}$ is the direct and reflected solar radiation force computed according to the LRA ray-surface interaction model (Equation (1) and (3)); $\mathbf{F}_{\text{sm}}$ is the direct and reflected solar radiation force computed according the SM ray-surface interaction model (Equations (1) and (2)); and m is the s/c mass.

3.3. Thermal re-radiation force model for multi-layer insulation (MLI) surfaces

For an MLI surface, the force arising from TRR effect,$\mathbf{F}_{\text{mli}}$, is computed according to:

$$\mathbf{F}_{\text{mli}} = -\frac{2A}{3c}\sigma\epsilon T_{\text{mli}}^4\hat{\mathbf{n}} \tag{6}$$

$$\mathrm{T}_{\text{mli}}^4 = \begin{cases} \frac{\alpha E\cos\theta+\epsilon_{\text{eff}}\sigma \mathrm{T}_{\text{sc}}^4}{\sigma(\epsilon_{\text{mli}}+\epsilon_{\text{eff}})} & ,-\frac{\pi}{2}<\theta<\frac{\pi}{2} \\ 0 & ,\text{otherwise} \end{cases} \tag{7}$$

where σ is the Stefan-Boltzmann constant; α is the absorptivity of the material; ϵ is the thermal emissivity of the material; ϵ_{eff} is the effective emissivity between the surface material and the s/c interior; T_{sc} is the internal temperature within the s/c bus; and all other terms are as previously defined. For details of the modelling assumptions used to derive Equations (6) and (7), see Adhya (2005).

3.4. OSR TRR force model

For OSR materials, the direct and reflected components of the solar radiation force are calculated using Equations (1) and (2), and the TRR component of the force,$\mathbf{F}_{\text{osr}}$, is computed according to:

$$\mathbf{F}_{\text{osr}} = \begin{cases} -\frac{2}{3}\alpha_{\text{osr}}W\hat{\mathbf{n}} & ,-\frac{\pi}{2}<\theta<\frac{\pi}{2} \\ 0 & ,\text{otherwise} \end{cases} \tag{8}$$

where α_{osr} is the absorptivity of the surface material and all other terms in Equation (8) are previously defined.

The OSR TRR model (Equation (8)) is most applicable to the radiators on the −Z face on the FOC s/c. All other radiators are not sun illuminated nominally. The model assumes that all absorbed solar radiation is instantly re-radiated as heat in a diffuse manner, and that absorbed solar radiation is the only source of heat flux through the radiators. Thus, it is an incomplete thermal force model. It does not consider the excess heat generated from onboard components (e.g., reaction wheels), the dissipation of this through the radiator panels, and the impact of this on the overall thermal balance. To some extent, we deal with these limitations in Sections 3.6 and 3.7.

3.5. Thermal force model for the Navigation antenna (NAVANT)

On the Galileo s/c, the NAVANT is mounted on the +z-panel of the bus. This is shown in Figs. 4 and 5 for IOV and FOC, respectively. The NAVANT surface is covered with a single-layer insulation (SLI) sunshield material and the NAVANT itself is thermally separated from +z-panel by an MLI blanket, as shown in Fig. 7. There is a thermistor, depicted by the red dot in Fig. 7, which logs temperature measurements at the NAVANT thermal reference point (TRP) as part of the telemetry stream.

For the thermal force model, in essence, we require the temperature of the NAVANT surface under all operating conditions. Thus, we considered it worthwhile to investigate whether the TRP thermistor readings are a useful source of information on this. First, we compared modelled TRP temperature values (from design simulations) against on-orbit TRP temperature measurements over several orbital periods. The simulated values were consistent with the on-orbit measurements, both in terms of magnitude and in terms of temperature variation patterns over the orbital cycle, suggesting that the on-orbit temperature observations are reliable and explicable. Then, SLI sunshield temperature values (from design simulations) were compared against on-orbit TRP temperature measurements, over the same period.

In full sunlight ($\theta < \frac{\pi}{2}$), the SLI temperatures are much higher (up to +80°C) than the observed TRP temperatures.

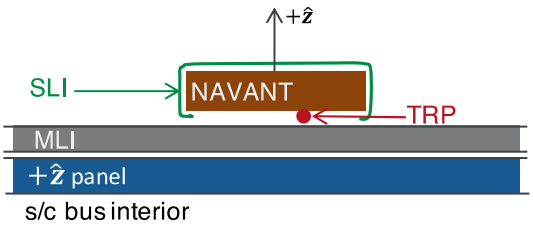

Fig. 7. An illustration of the NAVANT, which is mounted onto the +z surface of all Galileo s/c bus and is thermally separated from the s/c bus interior by an MLI blanket. The location of the thermal reference point (TRP) on the underside of the NAVANT unit is also indicated.

Also, the temperature variation patterns between the SLI sunshield and the TRP were different. We suspect this is due to differences in thermal inertia between the very-thin, very-light SLI material and the thick, heavy NAVANT unit on which the TRP is fixed. Thus, in full sunlight, the information provided by the TRP measurements is not suitable, by itself, for the NAVANT thermal force model. Our analysis suggests an OSR-type approach, where we assume all absorbed radiation is instantaneously re-radiated from the SLI surface, is more suitable.

Outside sunlight ($\theta > \frac{\pi}{2}$) and during eclipse, the temperature variation patterns between the SLI sunshield and the TRP were consistent, but with an offset of about −30°C in the SLI surface temperatures. Thus, the observed TRP measurements can provide useful information for the NAVANT thermal force model.

Based on these observations, for the Galileo s/c NAVANT surfaces, we compute the thermal force arising from the Galileo s/c NAVANT surface, $\mathbf{F}_{\text{nav}}$, according to:

$$\mathbf{F}_{\text{nav}} = \begin{cases} -\frac{2}{3}\alpha_{\text{sli}} W \hat{\mathbf{n}}, \theta < \frac{\pi}{2} \\ -\frac{2A}{3c}\sigma\epsilon_{\text{sli}}\left(\text{T}_{\text{trp}} - 30^{\circ}\right)^4 \hat{\mathbf{n}}, \text{otherwise and during eclipse} \end{cases} \tag{9}$$

where α_{sli} is the absorptivity of the SLI material; ϵ_{sli} is the emissivity of the SLI material; T_{trp} is the temperature according to the TRP thermistor; and all other terms are as previously defined. Fig. 8 reflects our understanding of the typical temperature variation pattern in the NAVANT surface over one orbit during eclipse season.

3.6. Thermal force model for the +x clock panel

On the Galileo s/c, the clock panel located on the interior of the +x-surface is temperature-stabilised. The temperature is monitored using thermistors and can be adjusted. As shown in Fig. 3, under normal operating conditions, the $+\hat{\mathbf{x}}$ direction remains in darkness at all times, and in this case the +x-surface temperature, $T_{+\text{x}}$, can be inferred from the clock panel temperature using $\text{T}_{(+\text{x})} = \text{T}_{\text{clk}}$-10°C. This approach was recommended by Guido Barbagallo, thermal engineer involved with the Galileo programme at ESTEC, based on experience. It allows us to account for the force arising due to heat generated by the clock panel being dissipated through the +x-surface, $\mathbf{F}_{\text{clk}}$, according to:

$$\mathbf{F}_{\text{clk}} = -\frac{2A_{\text{osr},+\text{x}}}{3c}\sigma\epsilon_{\text{osr}} T_{+\text{x}}^4 \hat{\mathbf{x}} \tag{10}$$

where $A_{\text{osr},+\text{x}}$ is the area of the radiator on the +x-surface; ϵ_{osr} is the emissivity of the OSR material on the +x-surface and all other terms are previously defined.

3.7. Asymmetric heat loss through the +Y and -Y radiators

For Galileo s/c following the nominal attitude laws, the sun does not shine on the +Y or −Y surfaces of the bus. To

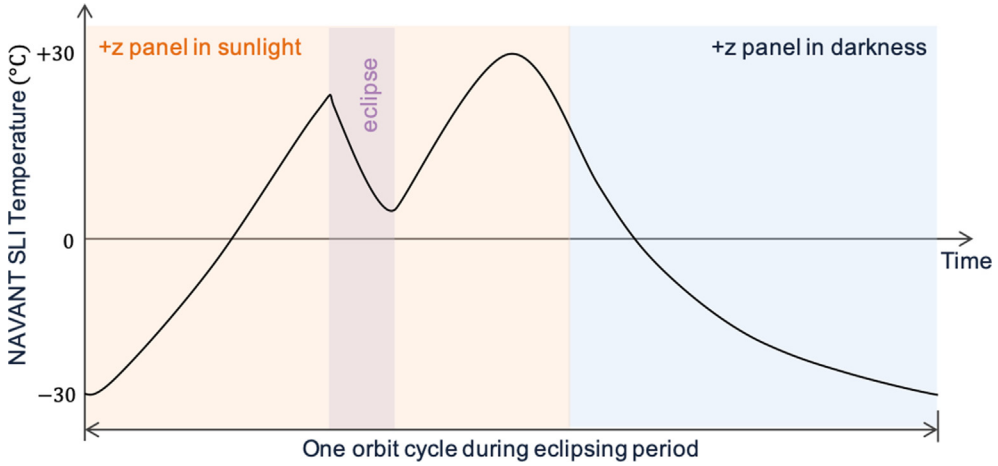

Fig. 8. A representative illustration of the NAVANT surface temperature model for the FOC spacecraft for a single orbit during eclipse season.

Table 1
Accelerations in the BFS $+\hat{y}$-direction arising from the asymmetric heat loss through radiators the $+Y$ *or* $-Y$ panels of the IOV and FOC spacecraft Units: nms^{-2}.

	IOV	FOC
Sunlight	−0.0294	−1.13
Eclipse	−0.222	−0.852

first order, this means that the $\hat{y}$ component, in the s/c BFS, of the solar (direct and reflected) force and of the TRR force should be negligibly small. However, in terms of radiation forcing more broadly, there should be a force in the BFS $\hat{y}$ direction caused by an imbalance in the heat lost through the radiators on the +Y and −Y surfaces. This effect was modelled by Guido Barbagallo, Galileo thermal engineer, using information about the power consumption of components on the +Y and −Y panels, during sunlight and eclipse conditions, for both IOV and FOC (G. Barbagallo 2010, personal communication, 19 March). The resulting accelerations are given in Table 1. In the FOC s/c, the size of this effect is relatively large, i.e., at the 10^{-9} ms^{-2} level. In the IOV s/c, the size of this effect is two orders of magnitude smaller at 10^{-11} ms^{-2} level during sunlight conditions and significantly larger during eclipse conditions at the 10^{-10} ms^{-2} level. The values in Table 1 are presented to give readers a sense of the relative magnitude of the Y-bias effect expected from the satellite design due to power dissipation. In our validation tests (Section 5), the Y-bias effect is estimated, and we do not use *a priori* values for this in the estimation process.

Other factors may contribute to the Y-bias effect, such as misalignment of the solar panels with respect to the s/c bus or a misalignment of sun sensor, although it is unlikely that these would affect the IOV and FOC spacecraft in a common way.

3.8. Analysis of the impact of the separate bus components in acceleration-space

In Fig. 9, we look at the theoretical impact of the modelling concepts introduced in Sections 3.2, 3.4, 3.6 and 3.7 by analysing the size and shape of their effect in the acceleration space. The independent variable is the Earth-Probe-Sun angle, θ'_{EPS}, as shown in Fig. 3, and it ranges from 0 to π. We use 700 kg for the mass of both the IOV and FOC s/c. The blue and orange curves use $\Delta\mathbf{a}_s$ (Equation (5)) values to show the impact of mismodelling the LRA surfaces as SM surfaces for IOV and FOC, respectively. The yellow curve uses Equation (8) and shows the impact of thermal re-radiation from the OSR panel on the −Z surface of the FOC bus. The green curve shows the impact of the thermal force caused by heat loss through the radiators on the +Y and −Y surfaces on the FOC bus, during full sunlight conditions. The corresponding value for the IOV s/c is given in Table 1, where the values for both IOV and FOC during eclipse conditions are also given. In our force modelling work, as a rule-of-thumb, we consider effects that result in accelerations at the 10^{-10} ms^{-2} level or greater to be significant. On that basis, our results suggest that the impact of all the effects shown in Fig. 9 are relevant and should be properly dealt with in applications demanding the highest levels of accuracy and precision.

4. The Galileo IOV and FOC models: Description and data sources

For both IOV and FOC, the geometric model of the bus is generated from information contained in the reduced geometric and mathematical thermal model (RGTMM) files that were supplied alongside the s/c thermal interface control documents (ICD). A python script was written to convert this information into the UCL s/c modelling for-

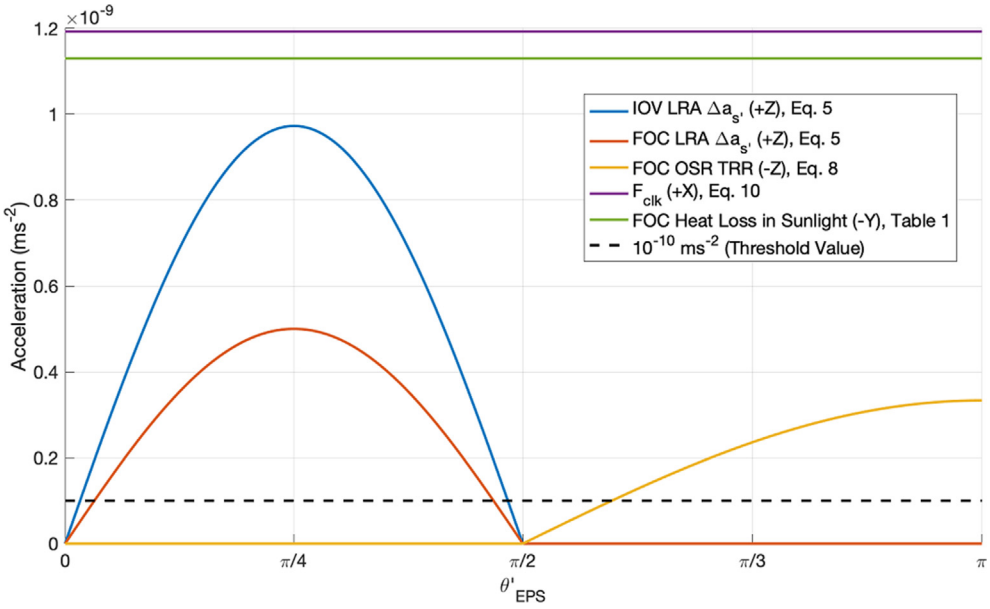

Fig. 9. Illustrating the size and shape of the impact of the modelling concepts introduced for this study in the acceleration space $\forall\theta'_{EPS}$ in the interval $(0, \pi)$. The black line indicates the threshold value of $10^{-10} ms^{-2}$. All effects above this line are significant and should be considered with care. The relevant surfaces, as defined in the s/c BFS, are indicated within parentheses.

Table 2
Surface material properties used for the IOV and FOC s/c models. As indicated within parentheses in Column 1, some materials are used in only one type of s/c (IOV or FOC) and others are used in both. The data sources are listed at the bottom on the table rather than in the bibliography because these are unpublished sources.

Surface Material Type with Description	Reflectivity (ν)	Specularity (μ)	Emissivity (ϵ)	Data Sources
Black MLI, Carbon-filled Kapton (IOV)	0.06	0	0.83	1,2
Silver MLI, Germanium-coated Kapton foil (IOV)	0.614	0.6	0.8	1,2
NAVANT Sunshield, Germanium-coated Kapton (IOV)	0.41	0.6	0.79	1,2
LRA, averaged over complete surface (Both)	0.962	0.9	0.83	2,4
OSR CMX 75-micron thickness (Both)	0.9	0.8	0.84	1,2
Black MLI, Carbon-filled Kapton (FOC)	0.07	0	0.83	2,3
NAVANT Sunshield (FOC)	0.488	0.6	0.79	2,3
[1] Galileo IOV – Space Segment: Satellite Thermal Interface Control Document for FM (GAL-ICD-ASTD-SA-R-0020)				
[2] Galileo IOV – Space Segment: Space Segment User Manual, Volume 6, Thermal (GAL-MAN-ASTD-SA-R-0008)				
[3] GalileoSat FOC: Thermal Interface Control Document (GS-THE-OHB-ICD-0010)				
[4] Meeting Notes, ESTEC, May 2017				

mat (Ziebart 2001, 2004), which was updated for this project to include additional material types, i.e. LRA and OSR types and to include additional material information, i.e. emissivity, at the component level. As a quality control check, the s/c models for IOV and FOC are examined in the UCL 3D spacecraft visualisation tool. This allows for zooming in and rotating around the s/c model to inspect the geometry and surface material information for any obvious errors. For example, the s/c models for IOV and FOC, as shown on the right side of Figs. 4 and 5, respectively, were verified against a variety of sources including computer renderings and cleanroom images.

The specific values used for the LRA, MLI, OSR and NAVANT surface coverings are given in Table 2, along with a description of the materials and the data sources. In some instances, there were inconsistencies in the values provided when comparing different sources, or the values given were at odds with our expectations (based on prior experience and understanding). For the most part, these issues were resolved through direct conversations with

thermal engineers with direct involvement in the development and operation of the Galileo mission at the European Space Research and Technology Center (ESTEC) in Noordwijk. A noteworthy difference between the IOV and FOC is that the FOC s/c has OSR material covering ~30% of the −z face and the IOV does not. Also, the exact amount of OSR material of the FOC +x face is known to vary across all the FOC satellites. This has not been taken into account in our modelling.

For the baseline UCL model, labelled UCL0, the bus model was produced using the UCL analytical SRP and TRR model Computation (STC) Software Version 5.7. All the other UCL bus models, as described in Section 5, were computed using the latest version of the UCL STC, Version 6.0, which supports new modelling computation strategies that allow for investigating the impact of the LRA solar force model (Equations (1) and (4)); the OSR TRR model (Equation (8)); the NAVANT model (Equation (9)); and can also deal with multiple MLI materials in the MLI TRR calculations. For both IOV and FOC, the bus model computation uses 10,000 spiral points; a pixel-array resolution of $1\,\mathrm{mm}^2$; the nominal s/c mass is 700 kg; and the reference value used for the solar irradiance at 1 astronomical unit (AU) is 1360.8 Wm^{-2} (Kopp et al. 2012).

For the box-wing (BW) s/c model, the geometry and the surface materials are mostly consistent with metadata published by the EUSPA at www.gsc-europa.eu/support-to-developers/galileo-satellite-metadata (accessed 4 October 2020). Differences include: the rear-side of the solar array (i.e. −Y side has only one surface material, as opposed to two for the front, with $\nu = 0.19$, $\mu = 0$); on the IOV +Z surface the area covered by the two surface materials is 1.72 and 1.28, as opposed to 1.01 and 1.99, for the black MLI and sunshield cover, respectively; the total FOC +Z face surface area is $3.168\,\mathrm{m}^2$ ($0.922\,\mathrm{m}^2, 2.246\,\mathrm{m}^2$) as opposed to $3.036\,\mathrm{m}^2$ ($1.053\,\mathrm{m}^2, 1.969\,\mathrm{m}^2$). The solar panel component of the BW model and the UCL models are identical. We model the solar panel contributions to SRP using Equations (1) and (2). We do not explicitly model thermal forces for the solar panels.

For the clock panel thermal force model (Equation (10)), we use the following values: $A_{\mathrm{osr},+x} = 0.88\mathrm{m}^2$; $\epsilon_{\mathrm{osr}} = 0.69$ and $T_{+x} = 50^{\circ}\mathrm{C}$. The values for $A_{\mathrm{osr},+x}$ and ϵ_{osr} are consistent with the published metadata. The $A_{\mathrm{osr},+x}$ value is known to be an overestimate because a portion of the OSR panel on the +x surface is covered by MLI. We suspect the value for ϵ_{osr} is an underestimate because our analysis of alternative data sources (Table 2) suggests a value of 0.84. The value for T_{+x} is too high. The s/c thermal ICD suggests T_{+x} is $\sim 10^{\circ}\mathrm{C}$during nominal operation. Thus, in our validation tests, we suspect that we may be overestimating the magnitude of the acceleration due to heat dissipation through by clock panel by $3 \times 10^{-10}\mathrm{ms}^{-2}$. This is significant and should be investigated further in future work. In (Sidorov et al. 2020), a value of 222 W power dissipation from the +X surface is proposed, based on based on assumed power requirements of instruments mounted on the +X panel. This value corresponds to $T_{+x} \sim 10^{\circ}\mathrm{C}$and is consistent with our analysis of the s/c thermal ICD. The value recommended by (Sidorov et al. 2020) for POD is 300 W, which corresponds to $T_{+x} \sim 32^{\circ}\mathrm{C}$.

To account for ERP, we use data from the Clouds and Earth Radiant Energy System (CERES; Wielicki et al. 1996) project, which is updated monthly, to model the shortwave (albedo) and longwave (infrared) components of the incoming Earth radiation flux at $10^{\circ} \times 10^{\circ}$ grid resolution in latitude and longitude. For the UCLx models, described in Section 5, we use the UCL bus models for the shortwave contribution to ERP and the BW model for the longwave contribution.

In our baseline antenna thrust model, we use values of 120 W and 250 W for signal power in the IOV and FOC s/c, respectively. These values are 15 W lower than the typical transmit power suggested by (Steigenberger et al. 2018) of 135 W for IOV and 265 W FOC. For the FOC s/c, in some of the model validation tests, we adjust the value of the signal power in the FOC antenna thrust to investigate the size of the unmodelled force due to heat emitted through the radiator panel on the -Z surface.

5. Model validation

The impact of the radiation force modelling concepts proposed in Section 3 were assessed in a POD analysis using Navigation Package for Earth Observation Satellites (NAPEOS), the GNSS data processing package used by the European Space Operations Centre (ESOC) in its contributions to the International GNSS Service (IGS; Johnston et al. 2017).

For these tests, the core data processing strategy follows, more or less, the approach used by ESOC in their POD processing for the IGS (http://navigation-office.esa.int/products/gnss-products/esa.acn, accessed on 28 September 2020), where the basic observables are undifferenced pseudoranges and carrier phases, with integer ambiguities resolved. The observations come from between 91 and 97 stations of the IGS Multi-GNSS Network (Montenbruck et al. 2017b), over the full two-year period, 2017 and 2018. The full orbit estimation procedure uses 24-hour batch processing, wherein each solution using observations from 00:00:00 to 23:59:30, but produces orbit estimates spanning the full 24-hr arc. Thus, between two consecutive 24-hour solutions, there is an overlap point at the midnight epoch. In this way, there are 730 completely independent orbit solutions with 729 overlap points considered in these tests. All active IOV and FOC satellites over the study period are included, with the exception of the four satellites 215–218, which came online on October

2018. The Earth gravity model is EIGEN-GLO5C up to degree and order 12 (Foerste et al. 2008) and the Jet Propulsion Laboratory (JPL) Development Ephemerides 405 (DE405) is used for third-body gravitational force modelling due to the Sun, Moon and other solar system planets. Solid Earth tides, ocean tides, solid Earth pole tide, ocean pole tide and general relativistic corrections are accounted for according to International Earth rotation and Reference systems Service (IERS) conventions (Petit and Luzum 2010). The numerical integrator is the Adams-Bashforth/Adams-Moulton 8th order prediction-correction multi-step method, as described in Springer (2009).

With the processing strategy fixed, this procedure is carried out six times with different orbit modelling strategies, which include:

- **ECOM2:** No *a priori* radiation force model, only the D4B1 Extended Empirical Code Orbit Model (Arnold et al. 2015) combined with a constrained three-parameter (constant, cosine and sine) along-track model that takes the argument of latitude as its argument.
- **BW + R:** Includes an *a priori* radiation force model that accounts for the solar force and the TRR force. Assumes all absorbed radiation is diffusely and instantaneously re-radiated. The Y-bias effect is included but switched off during eclipse periods. Details of the BW model of the s/c are given in Section 4. Also includes the ECOM-1 (Springer et al. 1999) and the along-track model as described above. The antenna transmit power for FOC is set to 0 W.
- **UCL0:** Same as BW + R, except that box component of the BW model is replaced by the bus model computed according to the process outlined in Bhattarai et al. (2019) using the UCL STC Version 5.7. In the s/c model, the surface materials belong to either the MLI or SM category, only. For materials in the SM category, the TRR effect is not accounted for. The antenna transmit power for FOC is set to 50 W.
- **UCL1:** Same as UCL0, except that the s/c model includes two additional material categories: LRA and OSR. The NAVANT covering is treated as an SM material and the thermal behaviour of the NAVANT is not considered. The bus model is computed using UCL STC Version 6.0.
- **UCL2:** Same as UCL1, but with the NAVANT thermal force model included (Equation (9)).
- **UCL2+:** Same as UCL2, but also including the clock panel thermal force model (Equation (10)) and the Y-bias effect (Table 1) is always on. The antenna transmit power for FOC is set to 20 W.

Table 3
Statistics of the day boundary discontinuities. Units are in mm. The smallest absolute values in each column are indicated in **bold**.

	Radial		Across-track		Along-track	
Galileo	Mean	STD	Mean	STD	Mean	STD
ECOM-2	−1.94	25.54	**0.12**	19.83	−1.92	27.42
BW + R	−1.14	22.78	0.34	18.51	−1.00	27.42
UCL0	**−0.40**	24.72	0.75	21.49	0.72	29.73
UCL1	−0.42	23.21	0.69	18.85	**0.23**	27.56
UCL2	−0.63	23.05	0.80	18.78	−0.74	27.15
UCL2+	−0.77	**22.31**	0.70	**17.49**	0.83	**26.80**
IOV						
ECOM-2	−4.33	26.33	**0.11**	21.76	−3.1	27.71
BW + R	−2.59	**23.17**	1.17	20.19	−1.34	27.26
UCL0	**−0.98**	27.5	1.40	24.63	**−0.18**	31.59
UCL1	−1.10	26.18	1.06	22.75	−1.11	30.78
UCL2	−1.30	26.16	1.15	22.95	−0.69	30.36
UCL2+	−1.60	23.40	1.34	**18.86**	−1.84	**27.22**
FOC						
ECOM-2	−1.40	25.36	**0.12**	19.36	−1.66	27.35
BW + R	−0.81	22.69	0.15	18.11	−0.93	27.46
UCL0	**−0.27**	24.04	0.58	20.71	0.93	29.29
UCL1	**−0.27**	22.47	0.61	17.85	**−0.27**	26.77
UCL2	−0.48	22.28	0.72	17.70	−0.75	**26.37**
UCL2+	−0.57	**22.05**	0.56	**17.16**	1.44	26.70

5.1. Internal consistency evaluation based on analysis of day boundary discontinuities

To assess the internal consistency of the orbits produced by the data processing strategies being tested, we compare the s/c position at the overlapping epoch (midnight) between two consecutive orbit solutions. The comparison is done by first computing the difference between the two solutions at the overlap point. This difference is the day boundary discontinuity (DBD) vector, which is then resolved into the radial (or height), across-track and along-track (HCL) components. The statistics of the HCL components of the DBDs are presented in Table 3. The top section provides the statistics for all Galileo s/c included in the analysis; the middle section provides statistics for the IOV s/c only; and the bottom section provides results for the FOC s/c only. For each s/c included in the analysis, there are 729 overlap points.

For the UCL class of models, the mean of the DBDs in each of the HCL components is below the 1 mm level for the FOC s/c and also for the Galileo s/c overall. For the IOV s/c, the mean value is below 1.5 mm. By this metric, the UCL2+ approach is a clear improvement over ECOM-2 and BW + R. Looking at the standard deviation of the DBDs, the broad pattern we observe is that there is a systematic improvement in the HCL components as more detailed effects are included in the modelling.

In Table 4, we show the percentage improvement in the standard deviation of the HCL components of the DBDs when the UCL2+ strategy is compared against the ECOM-2, BW + R, and UCL0 strategies. The UCL2+ shows an improvement over all three across all three components.

5.2. Orbit quality evaluation based on SLR residuals analysis

All Galileo satellites are equipped with an LRA mounted on the +z-surface. These are actively tracked by

Table 4
The percentage improvement in the standard deviation of the day boundary orbit discontinuities in the height, along-track and across-track components.

	UCL2+: Percentage change in the standard deviation of the day-boundary discontinuities		
	Radial (%)	Along-Track (%)	Across-Track (%)
ECOM-2	12.65	2.26	11.80
BW + R	2.06	2.26	5.51
UCL0	9.75	9.86	18.61

Table 5
Results of the SLR analysis based on the one-way range residuals for IOV and FOC (including the two eccentric satellites). The number of observations (No. Obs.) included in the analysis and the number of observations rejected as outliers (Obs. Rejected) are also indicated. The bias and standard deviation (STD) are given to the nearest mm. The smallest absolute values in the Bias and STD columns are indicated in **bold**.

Modelling strategy	IOV				FOC			
	Bias [mm]	STD [mm]	No. Obs.	Obs. Rejected	Bias [mm]	STD [mm]	No. Obs.	Obs. Rejected
ECOM-2	6	23	26,850	34	22	23	76,240	147
BW + R	−11	22	26,856	28	22	18	76,246	141
UCL0	−29	22	26,855	29	−15	21	76,258	129
UCL1	−21	22	26,856	28	−7	18	76,235	152
UCL2	−21	21	26,854	30	13	**17**	76,226	161
UCL2+	**0**	**17**	26,854	30	**−4**	**17**	76,215	172

the International Laser Ranging Service (ILRS; Pearlman et al. 2019). Thus, it is possible to evaluate the quality of Galileo orbit solutions using SLR – an accurate (particularly in the radial direction) and independent (optical) measurement technique. Our analysis of the SLR residuals includes all available observations over two full years, 2017 and 2018. The results of our analysis are given in Table 5, where we list the bias and standard deviation of the one-way range residuals alongside the number of observations included in the analysis and the number of those that were rejected. In the IOV and FOC cases, the UCL2 + model results in the smallest biases, 0mm and -4mm, respectively, and the smallest STD value of 17mm for both. For the FOC case, this result is achieved by reducing the antenna transmit power by 245 W when compared against the published value of 265 W (Steigenberger et al. 2018). This indicates that the overall impact of the unmodelled acceleration due to heat loss through the radiator on −Z surface is around the 10^{-9} ms^{-2} level.

6. Conclusions and discussion

A high-precision, physics-based radiation force modelling strategy was used to produce two new models, one for the Galileo IOV s/c and another for the Galileo FOC s/c. In both cases, the s/c bus surfaces are covered in material types, i.e., LRA, OSR, SLI and multiple MLI coverings, that were either not encountered or not specifically dealt with in earlier work. To address this, a number of modelling enhancements were proposed and tested, including: a specific model to account for the direct and reflected solar radiation force for LRA surfaces (Equations (1) and (4)); a design update of the bus model computation process to allow for more than one MLI material; a specific thermal force model for OSR surfaces (Equation (8)); a thermal force model for the NAVANT surface that includes a temperature model derived from on-orbit temperature measurements (Equation (9)); and force models to account for thermal emissions from radiator panels on the +X and ± Y surfaces for both IOV and FOC, and on −Z surface for FOC only.

Acceleration-domain analysis of the size and shape of the impact of the individual effects, as presented in Section 3.8, encouraged the development a successive series of models: BW + R, UCL0, UCL1, UCL2 and UCL2+, which were used to systematically investigate the influence of the new modelling concepts on orbit accuracy. This was done by analysing the results of a POD process that uses tracking measurements from all active Galileo s/c on-orbit, over two full years, 2017 and 2018, including during eclipse periods.

Broadly, our results show that very-detailed knowledge about the s/c (e.g., surface material properties) and its operations (e.g., thermal dissipation from surfaces) can and should be used to introduce physics-based concepts into the overall radiation force modelling strategy, and that doing this will systematically improve the orbit results. The highlight of this work is that the UCL2+ model, which incorporates all of the concepts described in Section 3, achieves one-way SLR residuals, to the nearest mm, of −4mm ± 17mm for FOC and 0mm ± 17mm for IOV.

These are encouraging results, however, there is room for improvement. There are several known limitations in the approach outlined here, which if addressed, could improve results even further. These include:

- **An incomplete and relatively simple thermal radiation force model**. The approach used in the UCL2+ model, as presented in Section 3, is not complete. To some extent, the excess heat generated from the on-board com-

ponents and the dissipation of this through the radiator panels is considered, e.g., Equation (10) for the clock panel on the +X surface and the approach for dealing with the asymmetric heat loss in the ± Y radiators (Section 3.7). However, on this aspect, the behaviour of the radiator of the −Z panel of the FOC s/c is not dealt with properly. This could be significant as it contributes directly to the uncertainty in the orbit scale and in any periodic forces in the $\hat{z}$ direction of the s/c BFS. With detailed knowledge of the heat lost through the s/c radiator panels (e.g., by inference based on information about the power consumption by the internal components), it should be possible to produce a more accurate and precise model of the thermal force overall. This is an area we are currently exploring at UCL.

- **Uncertainties in the surface material property information.** There are inconsistencies between surface material values published in the different design documents and operational manuals that were available as information sources for this study. Beyond this, there are discrepancies between those published values and reality. While the available data is sufficient for its original purpose, which is to inform the thermal design of the satellites, it can be improved further to support non-gravitational force modelling work. To address this issue, we recommend that samples of the exact surface materials on the Galileo s/c should be kept. These samples should be analysed for the purpose of determining the relevant surface material properties, and that information should be provided to GNSS researchers for the purpose of improving the force modelling, and consequently the overall orbit accuracy.
- Other factors that are not explicitly dealt with but could have an observable impact, such as the change of surface material characteristics due to ageing, s/c mass history, solar flux variations, etc.

The bus model grids for the UCL2+ models are available electronically in the supplementary material, along with resources to support implementation and further independent model validation efforts that we believe will lead to overall improvements in Galileo POD.

Declaration of Competing Interest

The authors declare that they have no known competing financial interests or personal relationships that could have appeared to influence the work reported in this paper.

Acknowledgements

This work was funded, in part, by the European Space Agency as a collaborative project between UCL, Positim and GMV to develop radiation force models for the Galileo spacecraft (AO/1-8118/14/NL/LF). The UCL contribution to this work was also supported by the UK Natural Environment Research Council (NE/K010816/1; Grant No. 157630). The authors acknowledge the International Laser Ranging Service (ILRS) for providing SLR observation data. The authors acknowledge the use of the UCL Myriad High Performance Computing Facility (Myriad@UCL), and associated support services, in the completion of this work. We would like to thank Guido Barbagallo and James Etchells, thermal engineers at ESTEC, and Frederic Bard, power engineer, for sharing their knowledge and experience on the relevant operational details about the Galileo satellites. The authors wish to thank three anonymous reviewers and the editors for valuable suggestions which have helped improve the paper.

Appendix A. Supplementary material

Supplementary data to this article can be found online at https://doi.org/10.1016/j.asr.2022.04.003.

References

Adhya, S., 2005. Thermal re-radiation modelling for precise prediction and determination of spacecraft orbits. PhD Thesis, University College London.

Arnold, D., Meindl, M., Beutler, G., et al., 2015. CODE's new solar radiation pressure model for GNSS orbit determination. J. Geod. 89, 775–791. https://doi.org/10.1007/s00190-015-0814-4.

Bar-Sever, Y., Kuang, D., 2003. New empirically-derived solar radiation pressure model for GPS satellites. JPL TRS 1992+.

Beutler, G., Brockmann, E., Gurtner, W., et al., 1994. Extended orbit modeling techniques at the CODE processing center of the international GPS service for geodynamics (IGS): theory and initial results. Manuscr. Geod. 19, 367–386.

Bhattarai, S., Ziebart, M., Allgeier, S., et al., 2019. Demonstrating developments in high-fidelity analytical radiation force modelling methods for spacecraft with a new model for GPS IIR/IIR-M. J. Geod. 93, 1515–1528. https://doi.org/10.1007/s00190-019-01265-7.

Bury, G., Zajdel, R., Sośnica, K., 2019. Accounting for perturbing forces acting on Galileo using a box-wing model. GPS Solut 23, art.74. https://doi.org/10.1007/s10291-019-0860-0.

Bury, G., Sośnica, K., Zajdel, R., Strugarek, D., 2020. Toward the 1-cm Galileo orbits: challenges in modeling of perturbing forces. J. Geod. 94, art.16. https://doi.org/10.1007/s00190-020-01342-2.

Cerri, L., Berthias, J.P., Bertiger, W.I., et al., 2010. Precision orbit determination standards for the Jason series of altimeter missions. Mar. Geod. 33, 379–418.

Darugna, F., Steigenberger, P., Montenbruck, O., Casotto, S., 2018. Ray-tracing solar radiation pressure modeling for QZS-1. Adv. Space Res. 62 (4), 935–943. https://doi.org/10.1016/J.ASR.2018.05.036.

Foerste, C.U., Flechtner, F., Schmidt, R., et al., 2008. EIGEN-GL05C - a new global combined high-resolution GRACE-based gravity field model of the GFZ-GRGS cooperation. In: Geophysical Research Abstracts. Vienna, Austria, p Vol. 10, Abstract No. EGU2008-A-06944.

Johnston, G., Riddell, A., Hausler, G., 2017. The international GNSS service. In: Teunissen, P.J.G., Montenbruck, O. (Eds.), Springer Handbook of Global Navigation Satellite Systems, First Edit. Springer International Publishing, Cham, Switzerland, pp. 967–982.

Kopp, G., Fehlmann, A., Finsterle, W., et al., 2012. Total solar irradiance data record accuracy and consistency improvements. Metrologia 49, S29–S33. https://doi.org/10.1088/0026-1394/49/2/s29.

Li, Z., Ziebart, M., Bhattarai, S., et al., 2018. Fast solar radiation pressure modelling with ray tracing and multiple reflections. Adv. Space Res. 61 (9), 2352–2365. https://doi.org/10.1016/j.asr.2018.02.019.

Montenbruck, O., Steigenberger, P., Hugentobler, U., 2015. Enhanced solar radiation pressure modeling for Galileo satellites. J. Geod. 89, 283–297. https://doi.org/10.1007/s00190-014-0774-0.

Montenbruck, O., Steigenberger, P., Darugna, F., 2017a. Semi-analytical solar radiation pressure modeling for QZS-1 orbit-normal and yaw-steering attitude. Adv. Space Res. 59 (8), 2088–2100. https://doi.org/10.1016/J.ASR.2017.01.036.

Montenbruck, O., Steigenberger, P., Prange, L., et al., 2017b. The Multi-GNSS Experiment (MGEX) of the International GNSS Service (IGS) – achievements, prospects and challenges. Adv. Space Res. 59 (7), 1671–1697. https://doi.org/10.1016/J.ASR.2017.01.011.

Pearlman, M.R., Noll, C.E., Pavlis, E.C., et al., 2019. The ILRS: approaching 20 years and planning for the future. J. Geod. 93, 2161–2180. https://doi.org/10.1007/s00190-019-01241-1.

Petit, G., Luzum, B. (Eds.), 2010. IERS Conventions (2010) (IERS Technical Note 36). Verlag des Bundesamts für Kartographie und Geodäsie, Frankfurt am Main.

Rodriguez-Solano, C.J., Hugentobler, U., Steigenberger, P., 2012. Adjustable box-wing model for solar radiation pressure impacting GPS satellites. Adv. Space Res. 49 (7), 1113–1128. https://doi.org/10.1016/J.ASR.2012.01.016.

Saff, E.B., Kuijlaars, A.B.J., 1997. Distributing many points on a sphere. Math. Intell. 19 (1), 5–11.

Shepard, D., 1968. A two-dimensional interpolation function for irregularly-spaced data. In: Proceedings-1968 ACM National Conference, pp. 517–524. doi: 10.1145/800186.810616.

Sibthorpe, A.J., 2006. Precision Non-Conservative Force Modelling For Low Earth Orbiting Spacecraft. PhD Thesis, University College London.

Sidorov, D., Dach, R., Polle, B., et al., 2020. Adopting the empirical CODE orbit model to Galileo satellites. Adv. Space Res. 66, 2799–2811. https://doi.org/10.1016/j.asr.2020.05.028.

Springer, T.A., Beutler, G., Rothacher, M., 1999. A new solar radiation pressure model for GPS satellites. GPS Solut. 2 (3), 50–62. https://doi.org/10.1007/PL00012757.

Springer, T., 2009. NAPEOS Mathematical Models and Algorithms. DOPS-SYS-TN-0100-OPS-GN, Issue 1.0, Nov 2009. Available from: <https://hpiers.obspm.fr/combinaison/documentation/articles/NAPEOS_MathModels_Algorithms.pdf>.

Steigenberger, P., Thoelert, S., Montenbruck, O., 2018. GNSS satellite transmit power and its impact on orbit determination. J. Geod. 92, 609–624. https://doi.org/10.1007/s00190-017-1082-2.

Urschl, C., Gurtner, W., Hugentobler, U., et al., 2005. Validation of GNSS orbits using SLR observations. Adv. Space Res. 36 (3), 412–417. https://doi.org/10.1016/j.asr.2005.03.021.

Wielicki, B.A., Barkstrom, B.R., Harrison, E.F., et al., 1996. Clouds and the Earth's Radiant Energy System (CERES): an earth observing system experiment. Bull. Am. Meteorol. Soc. 77 (5), 853–868. https://doi.org/10.1175/1520-0477(1996)077<0853:CATERE>2.0.CO;2.

Zelensky, N.P., Lemoine, F.G., Ziebart, M., et al., 2010. DORIS/SLR POD modeling improvements for Jason-1 and Jason-2. Adv. Space Res. 46 (12), 1541–1558. https://doi.org/10.1016/J.ASR.2010.05.008.

Ziebart, M., 2004. Generalized analytical solar radiation pressure modeling algorithm for spacecraft of complex shape. J. Spacecr. Rockets 41 (5), 840–848. https://doi.org/10.2514/1.13097.

Ziebart, M., Dare, P., 2001. Analytical solar radiation pressure modelling for GLONASS using a pixel array. J. Geod. 75, 587–599. https://doi.org/10.1007/s001900000136.

Ziebart, M., Adhya, S., Sibthorpe, A., et al., 2005. Combined radiation pressure and thermal modelling of complex satellites: algorithms and on-orbit tests. Adv. Space Res. 36 (3), 424–430. https://doi.org/10.1016/j.asr.2005.01.014.

Ziebart, M., Sibthorpe, A., Cross, P., et al., 2007. Cracking the GPS-SLR orbit anomaly. In: ION GNSS 2007. Fort Worth, Texas, pp. 2033–2038.

Ziebart, M., 2001. High precision analytical solar radiation pressure modelling for GNSS spacecraft. PhD Thesis, University of East London.